

Measurement of Ion Currents through Porous Membranes with Scanning Ion Conductance Microscopy

Chiao-Chen Chen, Maksymilian A. Derylo, and Lane A. Baker*

Department of Chemistry, Indiana University, 800 East Kirkwood Avenue, Bloomington, Indiana 47405

Scanning ion conductance microscopy (SICM) was used to interrogate ion currents emanating from nanometer-scale pores of a polymer membrane. The transport activity of individual pores was measured by examining ion current images and corresponding topographic images recorded simultaneously. Localized ion currents over individual nanopores were generated by introducing a concentration difference between the upper and lower chambers of a diffusion cell. To better estimate these localized ion currents, Goldman–Hodgkin–Katz (GHK) theory was used to model ion current through a permeable membrane under gradients of both concentration and applied potential. Experimental ion current profiles over a single pore fit well with theoretical plots calculated from the GHK model. On the basis of this analysis, nanoscale transport properties can be measured with SICM.

In this article, we report measurements of localized ion currents over the surface of porous membranes using scanning ion conductance microscopy (SICM). The transport of ions plays key roles in a diverse number of fields. For instance, ion transport through cell membranes in living systems is critical for biological function. Similarly, the transport of ions (in the form of protons) through selective membranes in fuel cells is an important factor in future sources of energy. To study ion transport, macroscopic measurements averaged over large areas, such as bulk measurements of electrical conductivity, may be used. In selected settings, microscopic measurements, such as electrophysiological recordings which make use of the patch-clamp technique, can also be employed. The use of SICM affords the opportunity to measure ion currents with nanometer-scale spatial resolution for these important fields of study. Measured ion currents can also be correlated simultaneously with heterogeneous surface topography, offering additional insight into relationships between surface structure and transport activity.

To date, several key investigations of localized ion transport through porous membranes have been reported. These former studies are based primarily on scanning electrochemical microscopy (SECM). SECM is capable of collecting both electrochemical and topographic information of a sample when immersed into a redox-active solution.^{1–7} The first demonstration of imaging local permeability with SECM was performed by measuring transport

of electroactive species from pore openings of a mica membrane.⁸ Further applications utilizing SECM to study ion transport pathways in synthetic and biological membranes,^{9–12} as well as determinations of diffusion, migration, and convection currents through nanoscale pores, have also been reported.^{11,13–16}

Although insightful, standard SECM instruments suffer from limitations.¹⁷ The feedback loop^{4,5} of typical SECM instruments requires the presence of a redox-active mediator. This redox mediator can interfere with the processes being measured, e.g., physiological function. The feedback loop is also slow and is not generally useful for dynamic feedback and tip positioning while scanning. Also, when recorded as a function of tip position, the current response of SECM may be a convolution of both the topography and the electrochemical reactivity of the substrate. Advances in SECM instrumentation, such as alternating current scanning electrochemical microscopy (AC-SECM),^{18,19} tip position modulation scanning electrochemical microscopy (TPM-SECM),²⁰ and scanning electrochemical atomic force microscopy (SECM-AFM),²¹ have been introduced to remedy some of these shortcomings.^{18,19} With these methodologies, a limited number of attempts to correlate surface topography and local mass

- (1) Engstrom, R. C.; Meaney, T.; Tople, R.; Wightman, R. M. *Anal. Chem.* **1987**, *59*, 2005–2010.
- (2) Bard, A. J.; Fan, F. R. F.; Kwak, J.; Lev, O. *Anal. Chem.* **1989**, *61*, 132–138.
- (3) Husser, O. E.; Craston, D. H.; Bard, A. J. *J. Electrochem. Soc.* **1989**, *136*, 3222–3229.
- (4) Kwak, J.; Bard, A. J. *Anal. Chem.* **1989**, *61*, 1794–1799.
- (5) Kwak, J.; Bard, A. J. *Anal. Chem.* **1989**, *61*, 1221–1227.
- (6) Mandler, D.; Bard, A. J. *J. Electrochem. Soc.* **1989**, *136*, 3143–3144.
- (7) Kwak, J. Y.; Lee, C.; Bard, A. J. *J. Electrochem. Soc.* **1990**, *137*, 1481–1484.
- (8) Scott, E. R.; White, H. S.; Phipps, J. B. *J. Membr. Sci.* **1991**, *58*, 71–87.
- (9) Macpherson, J. V.; Ohare, D.; Unwin, P. R.; Winlove, C. P. *Biophys. J.* **1997**, *73*, 2771–2781.
- (10) Tsionsky, M.; Zhou, J. F.; Amemiya, S.; Fan, F. R. F.; Bard, A. J.; Dryfe, R. A. W. *Anal. Chem.* **1999**, *71*, 4300–4305.
- (11) Bath, B. D.; White, H. S.; Scott, E. R. *Pharm. Res.* **2000**, *17*, 471–475.
- (12) Uitto, O. D.; White, H. S. *Anal. Chem.* **2001**, *73*, 533–539.
- (13) Scott, E. R.; White, H. S.; Phipps, J. B. *Anal. Chem.* **1993**, *65*, 1537–1545.
- (14) Bath, B. D.; Lee, R. D.; White, H. S.; Scott, E. R. *Anal. Chem.* **1998**, *70*, 1047–1058.
- (15) Bath, B. D.; White, H. S.; Scott, E. R. *Anal. Chem.* **2000**, *72*, 433–442.
- (16) Uitto, O. D.; White, H. S.; Aoki, K. *Anal. Chem.* **2002**, *74*, 4577–4582.
- (17) Bauermann, L. P.; Schuhmann, W.; Schulte, A. *Phys. Chem. Chem. Phys.* **2004**, *6*, 4003–4008.
- (18) Ervin, E. N.; White, H. S.; Baker, L. A. *Anal. Chem.* **2005**, *77*, 5564–5569.
- (19) Ervin, E. N.; White, H. S.; Baker, L. A.; Martin, C. R. *Anal. Chem.* **2006**, *78*, 6535–6541.
- (20) Wipf, D. O.; Bard, A. J. *Anal. Chem.* **1992**, *64*, 1362–1367.
- (21) Macpherson, J. V.; Unwin, P. R. *Anal. Chem.* **2000**, *72*, 276–285.

* To whom correspondence should be addressed. E-mail: lanbaker@indiana.edu. Phone: 812-856-1873. Fax: 812-856-8300.

transport across track-etched nanopore membranes have been reported.^{21–23}

In addition to the aforementioned SECM-based techniques, SICM²⁴ is a promising tool to study localized ion transport and nanoscale conductance.²⁵ The SICM probe is composed of a nanopipette filled with a conductive electrolyte. When an electrode placed inside the nanopipette (probe) is biased relative to an external electrode in the bath solution, an ion current is generated. The nanopipette is then brought in close proximity to the surface of a sample of interest. As the nanopipette approaches the sample surface, the flow of ions through the tip opening is impeded (at distances approximately one radius of the tip opening²⁵), creating a reduction in the measured ion current. By monitoring the change in ion current as a function of probe position, a sensitive ion current-based feedback loop is created. This feedback loop provides SICM with accurate control of probe–sample separation, thus preventing damage to delicate surface features in a noncontact imaging mode.^{24,26,27} Furthermore, with the development of distance-modulated feedback protocols by the groups of Korchev and Klenerman, robust control over the tip–sample separation is attained.²⁸ These attributes make SICM especially well-suited for investigating nonconductive or biological materials in ionic solutions.²⁵

In the initial description of SICM by Hansma et al., an image based on ion current was reported for a nucleopore membrane.²⁴ Since this preliminary report, a number of studies have sought to capitalize on the attributes of SICM for ion current measurements. Consideration of ion currents measured while scanning with SICM has been described as related to biological ion channels.²⁹ Several key studies related to SICM operated in a so-called “smart patch-clamp” mode have also been reported.^{30–32} Finally, a tapping-mode SICM constructed by combining the feedback loop principles of AFM and SICM has successfully imaged the topography of a nucleopore membrane while simultaneously measuring the local conductivity of individual pores.³³ To date, however, a systematic study of ion currents with SICM has not been reported.

Herein, we describe the utilization of SICM to study localized ion transport through nanometer-scale porous membranes, with

an effort toward quantitatively evaluating ion currents. When operated with distance-modulated feedback, SICM records not only sample topography but can also simultaneously record local ion currents through individual pores. From these results, we conclude SICM provides an exceptional tool for measuring ion transport pathways and holds promise in further quantitative analysis of transport pathways in both biological membranes and nanoscale porous materials.

EXPERIMENTAL SECTION

Chemicals and Materials. All solutions were prepared using 18 M Ω ·cm H₂O from a Milli-Q water purification system (Millipore Corp., Danvers, MA). Potassium chloride (Mallinckrodt, Philipsburg, NJ) solutions with concentrations ranging from 0.1 to 4.0 M were used as electrolytes for SICM measurements. Potassium iodide (Mallinckrodt, Philipsburg, NJ) and sodium hypochlorite (13% active chlorine, Acros, Morris Plains, NJ) were used to prepare nanopore membranes.

Membrane Preparation and Characterization. Membranes were prepared through the track-etch process.³⁴ In this method, a polymer film is irradiated with heavy ions from a nuclear reactor or particle accelerator. These heavy ions create damage tracks which are susceptible to chemical etchants at an accelerated rate relative to the bulk polymer film. When the ion-tracked film is exposed to a chemical etchant (specific to the polymer material), a nanopore is created for every damage track that was present initially. Pore dimensions and diameters can be controlled by different etching conditions, including pH, temperature, time, and concentration of etchant. In this report, ion-tracked polyimide membranes (polyimide, 10⁶ tracks/cm², thickness 25 μ m, it4ip, Belgium) were immersed in 13% sodium hypochlorite solution at 70 °C to prepare membranes containing cylindrical nanopores. By controlling the time of etch, 5 and 10 min used here, membranes with two different pore diameters were obtained. After etching, membranes were washed with water and placed in 1 M potassium iodide solution for 30 min to neutralize residual etchant. Membranes were then rinsed with Milli-Q water and stored dry. Pore diameters were characterized with scanning electron microscopy (SEM, JEOL 5800 LV). Tapping-mode atomic force microscopy (AFM, Agilent 5500) was also used for comparison to SICM. Membranes were imaged in situ using NSC15/AIBS series cantilevers (Mikromasch USA, San Jose, CA) with nominal spring constants of 40 N/m and resonant frequency of 325 kHz. AFM images were subsequently analyzed with Gwyddion (David Nečas and Petr Klapetek, Brno, Czech Republic).³⁵ Statistical analysis of pore sizes was performed on grayscale images using ImageJ (National Institutes of Health, MD).³⁶

Instrumentation. Data was acquired using a ScanIC scanning ion conductance microscope (ionscope, London, U.K.) in conjunction with an Axopatch 200B current amplifier (Molecular Devices, Union City, CA). To perform experiments, a nanopore membrane was mounted in a diffusion cell (Figure 1). To generate a current of ions through the pores of the membrane, KCl concentrations in the bottom chamber were varied from 0.1 to 4.0 M, while the

- (22) Macpherson, J. V.; Jones, C. E.; Barker, A. L.; Unwin, P. R. *Anal. Chem.* **2002**, *74*, 1841–1848.
- (23) Gardner, C. E.; Unwin, P. R.; Macpherson, J. V. *Electrochem. Commun.* **2005**, *7*, 612–618.
- (24) Hansma, P. K.; Drake, B.; Marti, O.; Gould, S. A. C.; Prater, C. B. *Science* **1989**, *243*, 641–643.
- (25) Ying, L. M.; Bruckbauer, A.; Zhou, D.; Gorelik, J.; Shevchuk, A.; Lab, M.; Korchev, Y.; Klenerman, D. *Phys. Chem. Chem. Phys.* **2005**, *7*, 2859–2866.
- (26) Korchev, Y. E.; Bashford, C. L.; Milovanovic, M.; Vodyanov, I.; Lab, M. J. *Biophys. J.* **1997**, *73*, 653–658.
- (27) Korchev, Y. E.; Milovanovic, M.; Bashford, C. L.; Bennett, D. C.; Sviderskaya, E. V.; Vodyanov, I.; Lab, M. J. *J. Microsc. (Oxford)* **1997**, *188*, 17–23.
- (28) Shevchuk, A. I.; Gorelik, J.; Harding, S. E.; Lab, M. J.; Klenerman, D.; Korchev, Y. E. *Biophys. J.* **2001**, *81*, 1759–1764.
- (29) Shevchuk, A. I.; Frolenkov, G. I.; Sanchez, D.; James, P. S.; Freedman, N.; Lab, M. J.; Jones, R.; Klenerman, D.; Korchev, Y. E. *Angew. Chem., Int. Ed.* **2006**, *45*, 2212–2216.
- (30) Dutta, A. K.; Korchev, Y. E.; Shevchuk, A. I.; Hayashi, S.; Okada, Y.; Sabirov, R. Z. *Biophys. J.* **2008**, *94*, 1646–1655.
- (31) Gorelik, J.; Gu, Y. C.; Spohr, H. A.; Shevchuk, A. I.; Lab, M. J.; Harding, S. E.; Edwards, C. R. W.; Whitaker, M.; Moss, G. W. J.; Benton, D. C. H.; Sanchez, D.; Darszon, A.; Vodyanov, I.; Klenerman, D.; Korchev, Y. E. *Biophys. J.* **2002**, *83*, 3296–3303.
- (32) Siwy, Z.; Gu, Y.; Spohr, H. A.; Baur, D.; Wolf-Reber, A.; Spohr, R.; Apel, P.; Korchev, Y. E. *Europhys. Lett.* **2002**, *60*, 349–355.
- (33) Proksch, R.; Lal, R.; Hansma, P. K.; Morse, D.; Stucky, G. *Biophys. J.* **1996**, *71*, 2155–2157.

(34) Fleischer, R. L.; Price, P. B.; Walker, R. M., Eds. *Nuclear Tracks in Solids*; University of California Press: Berkeley, CA, 1975.

(35) <http://gwyddion.net>, accessed May 6, 2009.

(36) <http://rsbweb.nih.gov/ij/index.html>, accessed May 6, 2009.

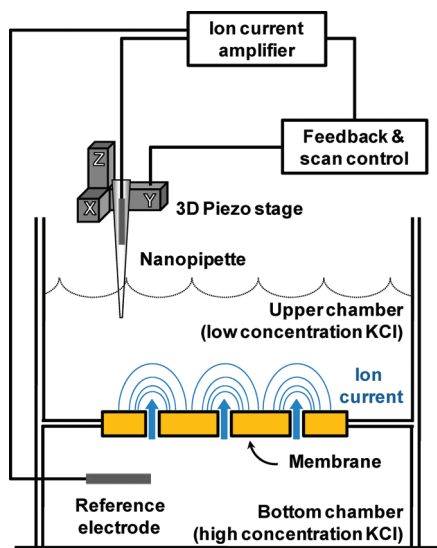


Figure 1. Schematic diagram of the scanning ion conductance microscope (SICM) and the diffusion cell used.

KCl concentration in the nanopipette and upper chamber was held constant at 0.1 M. Nanopipettes were fabricated routinely from glass capillaries (borosilicate glass, inner diameter 0.58 mm, outer diameter 1.0 mm, Sutter Instrument, Novato, CA) using a CO₂-laser-based pipette puller (P-2000, Sutter Instrument, Novato, CA). The tip openings of pipettes used here (nominally referred to as nanopipettes) have an inner diameter of ~ 150 nm and an outer diameter of ~ 700 nm, as characterized by SEM (see the Supporting Information).

One Ag/AgCl electrode was placed inside of a nanopipette mounted on the SICM scanner, and a second Ag/AgCl electrode was placed in the external bath solution. A potential difference of 100 mV was applied between the SICM probe and the reference electrode, and the ion current through the nanopipette opening was measured. When filled with 0.1 M KCl and lowered into the 0.1 M KCl bath solution, nanopipettes typically produced measured resistances of ~ 100 M Ω (see the Supporting Information). The nanopipette probe was mounted on the SICM scanner, and the vertical position was modulated 100 nm at 800 Hz, producing a distance-modulated ion current, which was amplified and sent to the feedback and scan control system. After approach to the sample surface, the nanopipette was raster scanned over the surface of the sample in the x and y dimensions. The lateral and vertical positions of the nanopipette and the magnitude of dc ion current were measured, producing both topographic and dc current images, respectively.

Membranes were masked in clear tape with a 1 mm diameter through-hole which exposed the porous membrane to electrolyte solutions on both sides (Figure 1). Topographic representations of the membrane surface were recorded by measuring the z -piezo displacement required to keep a constant probe-sample separation, which is dictated by the modulated (ac) component of the measured ion current. As described by Shevchuk et al.,²⁸ distance modulation maintains a relatively constant probe-sample separation even in the case of changes in local conductivity or instrument drift. Ion currents measured at the membrane surface were recorded through the nonmodulated (dc) component of the ion current, as recorded directly from a current amplifier. SICM

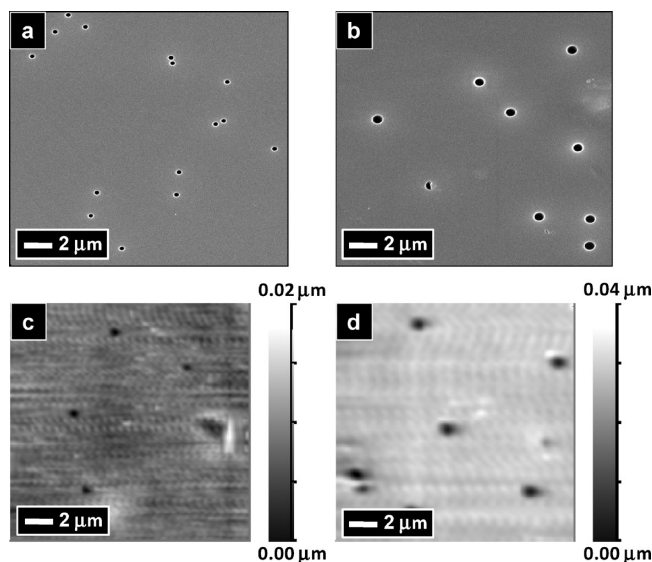


Figure 2. Topographic images of porous polyimide membranes taken by SEM (a and b) and SICM (c and d) after 5 (a and c) and 10 (b and d) min of chemical etching. (Panels a and c are taken from the same membrane (5 min etched). Panels b and d are taken from the same membrane (10 min etched). In both cases, images shown are collected from different areas of the membrane of interest.)

images were analyzed with SICM Image Viewer (ionscope, London, U.K.) and Gwyddion.³⁵

RESULTS AND DISCUSSION

Membrane Topography. Porous polyimide membranes with two different pore sizes were prepared through the track-etched method by immersing ion-tracked polymer films in a solution containing 13% sodium hypochlorite at 70 °C for 5 and 10 min, respectively. SEM images were taken to standardize the pore sizes of the etched membranes and to correlate the topographic images of these samples recorded with SICM. Figure 2 shows typical secondary electron SEM images and SICM topographic images of 5 (Figure 2, panels a and c) and 10 min (Figure 2, panels b and d) etched membranes. SICM images (Figure 2, panels c and d) were taken with the instrumental setup described in the Experimental Section, in which both the upper and lower chambers of the diffusion cell were filled with 0.1 M KCl.

From SEM images, average pore diameters of 272 ± 9 nm ($n = 22$) for the 5 min etched membrane and 535 ± 40 nm ($n = 34$) for the 10 min etched membrane were determined. Analyzing SICM data gave average pore diameters for 5 and 10 min etched membranes as 1.16 ± 0.21 μm ($n = 58$) and 1.49 ± 0.15 μm ($n = 32$), respectively, significantly larger than measurements obtained by SEM. Atomic force microscopy was used to provide additional comparison in the measured pore diameter. Pore diameters measured by AFM are 0.68 ± 0.05 μm ($n = 43$) and 1.17 ± 0.15 μm ($n = 55$) for 5 and 10 min etched membranes, respectively, which are intermediate to measurements recorded using SEM and SICM. Distributions of pore width measurements recorded by SEM, AFM, and SICM are shown in Figure 3.

Convolution is a well-known artifact often present in proximal probe techniques, which is obviously not observed in electron microscopy.³⁷ Convolution of the observed image between a probe and sample is further exacerbated when the size of the probe approaches the size of the sample feature being imaged, as

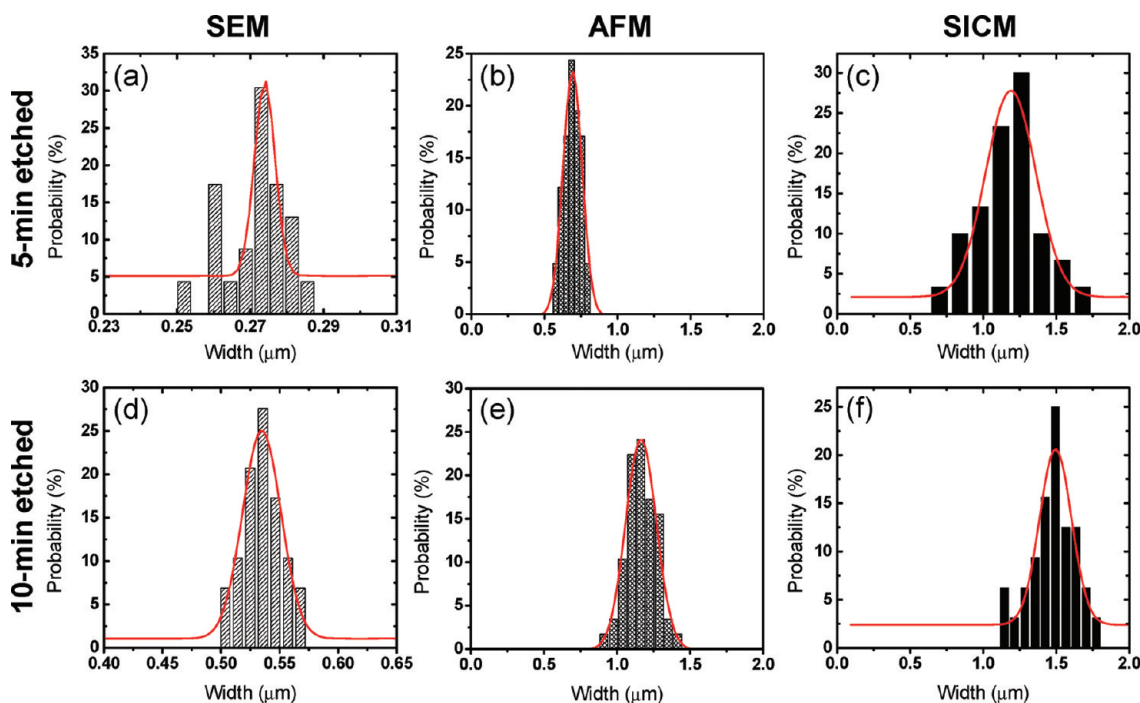


Figure 3. Pore diameters of a 5 min etched membrane measured by (a) SEM, (b) AFM, and (c) SICM and pore diameters of a 10 min etched membrane measured by (d) SEM, (e) AFM, (f) and SICM.

encountered here. For SICM, the resolution of images recorded may also be significantly influenced by both the inner and outer diameters of the nanopipette. Nanopipettes with smaller inner diameter typically give higher resolution images (even to the level of individual proteins²⁹), but overall currents measured may be diminished significantly. Nanopipettes with intermediate inner diameters (~ 150 nm) were employed in this report to compromise between acceptable resolution and adequate ion current values.

In addition to the nanopipette geometry, in the case of ion currents imaged with SICM as described in this report, the distance between the nanopore membrane surface and the nanopipette probe allows for diffusion of current-carrying ions away from the true membrane pore opening. This effectively broadens the feature imaged, in agreement with the data recorded and modeled current profiles described further below. Taking SEM to be the more accurate representation of the true pore diameter and to facilitate further discussion, 5 and 10 min etched membranes are hereafter referred to as 300 and 500 nm diameter nanopore membranes, respectively, based on measurements from SEM images.

Imaging Ion Currents with SICM. In addition to topographic images, ion transport activity of individual pores may also be interrogated by recording the magnitude of transmembrane ion current with SICM. Figure 4 shows a topographic and the corresponding ion current image of the 500 nm diameter nanopore membrane when the nanopipette and the upper and lower chambers of the diffusion cell were filled with 0.1 M KCl. From the topographic image, four track-etch pores are present (denoted by arrows), with apparent diameters which range from 1.36 to 1.55 μm . A larger feature (denoted by a dashed circle) with a diameter of $\sim 3.25 \mu\text{m}$ is observed in the center of the image. From

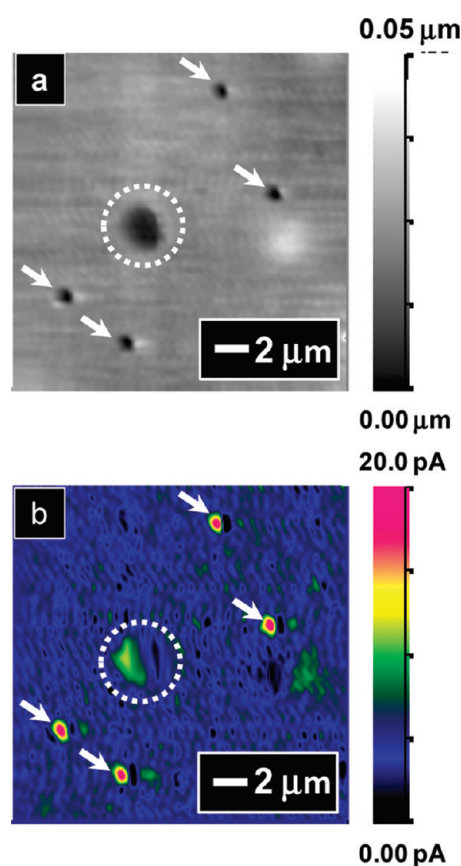


Figure 4. (a) Topographic and (b) the corresponding ion current image of the 500 nm diameter nanopore membrane recorded simultaneously with SICM. A potential difference of 100 mV is applied between the SICM probe and bath solution. The region circled in the topographic image corresponds to a feature which is not a pore; arrows point to features which are pores.

(37) Shevchuk, A. I.; Hobson, P.; Lab, M. J.; Klenerman, D.; Krauzewicz, N.; Korchev, Y. E. *Biophys. J.* **2008**, *94*, 4089–4094.

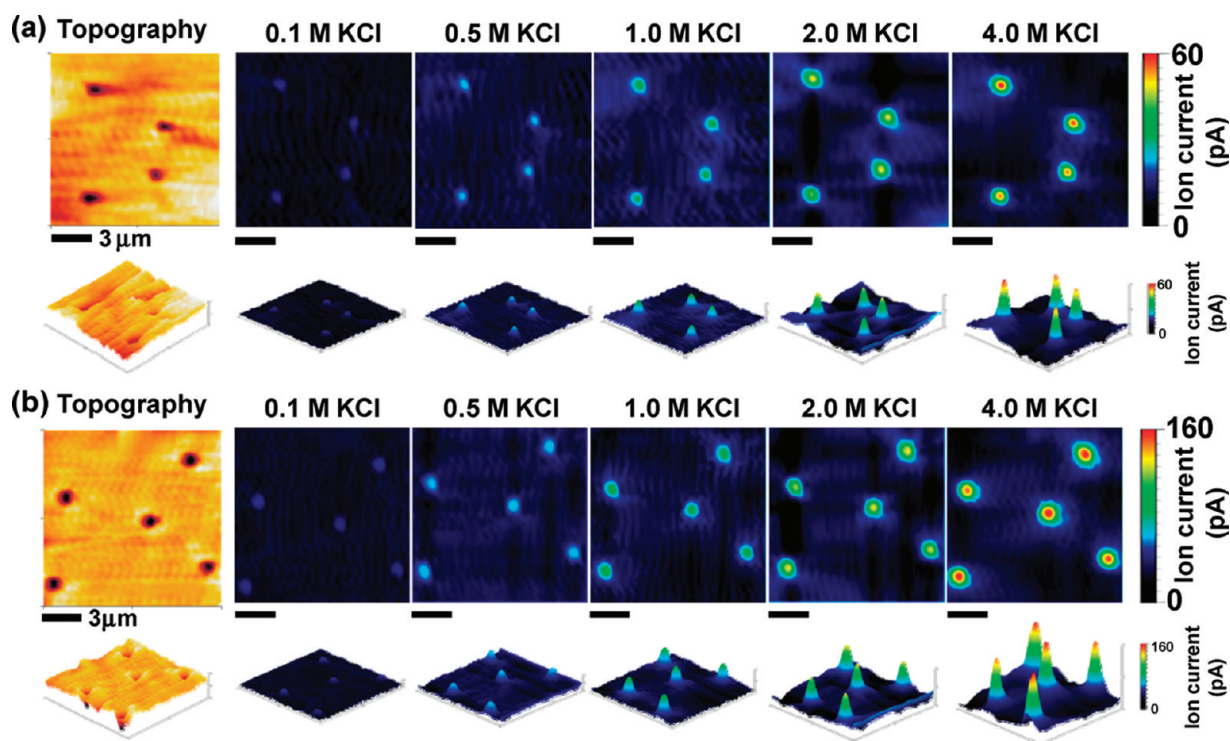


Figure 5. Topographic and ion current images of (a) a 300 nm diameter nanopore membrane and (b) a 500 nm diameter nanopore membrane as a function of the KCl concentration in the lower chamber (concentration indicated above each image). For all images, the electrolyte in the upper chamber of the diffusion cell is maintained at 0.1 M KCl.

the ion current image, only the four pores show ion transport activity, producing nominal ion currents of ~ 20 pA. The large central feature indicated with a dashed circle does not display significant transport activity, suggesting this feature is a variation in the topography of the membrane but does not represent an actual transmembrane pore. The differences in features observed between topographic and ion current images demonstrate the capability of SICM in discerning transport pathways for porous materials with heterogeneous surface features.

Effects of a Transmembrane Concentration Difference on the SICM Current Images. We introduce a transmembrane concentration difference between the upper and lower chambers of the diffusion cell by altering the concentration of KCl in the lower chamber with values ranging from 0.1 to 4.0 M, while maintaining the KCl concentration in the upper chamber at 0.1 M. This concentration difference creates a transmembrane ion current as KCl diffuses from the lower chamber (high concentration) to the upper chamber (low concentration) of the diffusion cell.

Figure 5 displays images recorded for topography and ion current of both the 300 nm diameter (Figure 5a, top) and 500 nm diameter (Figure 5b, bottom) nanopore membrane. Topographic images (far left) for each membrane along with two- and three-dimensional ion current images measured at each transmembrane concentration difference are shown. For all ion current images, the KCl concentration in the upper chamber of the diffusion cell was 0.1 M; the concentration of KCl in the lower chamber is indicated above each respective image. Changes in the transmembrane concentration difference produce no significant variation in topographic images, but obvious differences are observed in the recorded ion current images.

From the ion current images of the 300 nm diameter nanopore membrane (Figure 5a), when there is no concentration difference between the lower and upper chamber, the peak value of the measured ion current is small (~ 7 pA). The greatest transmembrane ion currents measured for the 300 nm diameter nanopore membrane are nominally 55 pA under a KCl concentration difference of 0.1 M (upper chamber) – 4.0 M (lower chamber). Ion currents measured for the 500 nm diameter nanopore membrane present the same trend—the higher the transmembrane concentration difference, the larger the measured ion current emanating from the membrane pores. A plot of the peak value of the ion current as a function of the concentration of KCl solution in the lower chamber affords a linear relationship, as shown in Figure 6. Linear regression yields correlation coefficients (R^2) which are all larger than 0.96, demonstrating reasonable agreement between the transmembrane concentration difference and the magnitude of the measured ion current.

For any set of transmembrane concentrations of KCl used, e.g., 0.1 M (upper chamber) – 0.1 M (lower chamber), 0.1 M (upper chamber) – 0.5 M (lower chamber), etc., ion currents measured for the 500 nm diameter nanopore membrane were always larger than those measured for the 300 nm diameter nanopore membrane (Figure 6 and Table 1). Measured differences in transmembrane ion currents are fundamentally related to the mass-transfer resistance determined by the pore structure.⁸ The resistance of a pore decreases when the pore diameter becomes larger or the pore length becomes shorter. Obviously, the 500 nm diameter nanopore membrane has pores with larger diameter than those of the 300 nm diameter nanopore membrane. According to the cross-sectional SEM images of these two membranes, the pore length (i.e., membrane thickness) of 500 nm diameter nano-

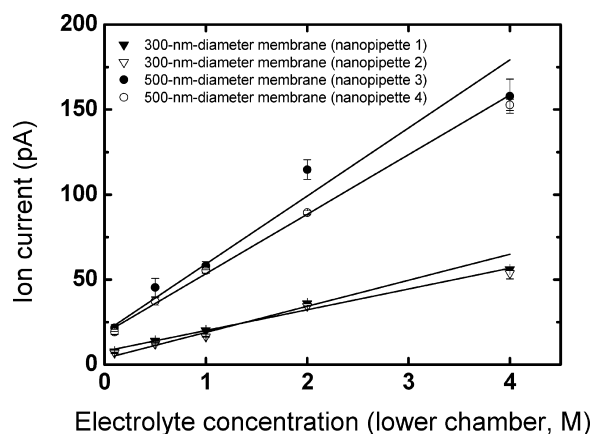


Figure 6. Dependence of the peak ion current on the lower-chamber KCl concentration for a 300 nm diameter nanopore membrane (▼ and ▽) and a 500 nm diameter nanopore membrane (● and ○). Results from two different nanopipettes are shown for each membrane.

pore membrane, 11.03 μm , is also shorter than the pore length of the 300 nm diameter nanopore membrane, 12.67 μm . This difference in membrane thickness arises from etching of the bulk polymer films during pore formation. Since the 500 nm diameter nanopore membrane was etched longer to create larger pores, the bulk membrane material was also etched to a greater degree, causing a thinner membrane.

Multiple nanopipettes were used in these experiments, and subtle variations in the geometries of the nanopipettes obtained result in differences in the overall nanopipette conductivity (and the subsequent ion current recorded); however, the trends observed are consistent for a given nanopipette. To illustrate this point, results from two different nanopipettes are reported in Table 1 for each membrane examined.

Measurements of mass transport using SECM have demonstrated that for constant probe–sample separations, the flux of redox mediator through a pore in the membrane is directly proportional to the current (faradaic current from redox species) measured at the microelectrode probe regardless of the mode of transport, convection, diffusion, or migration. SICM differs from SECM, as instead of measuring the faradaic current from a redox mediator, the ionic current carried by the electrolyte is measured directly. Quantitative analysis of ion currents—whether the ion is redox-active or not—through a pore may therefore be made using SICM.

Physical perturbations of ions diffusing from pores in the membrane by the SICM probe must also be considered. In any effort to evaluate the results of such experiments, care must be taken to ensure the tip operates in a noninteracting regime. The criterion of a noninteracting probe requires that the diffusion field of ions translocating a pore in the membrane cannot be perturbed significantly by the nanopipette probe; otherwise, the transmembrane current measured, which is determined directly by the diffusion field of translocating ions, will be altered. Previous reports have shown that for certain probe–sample separations, a proximal probe can operate in a noninteracting regime.^{8,13} At these distances, the spatial variation in the concentration profile is large relative to the size of the tip of the nanopipette. As derived by Scott et al.,¹³ the probe–sample distance, d , which satisfies this

criterion can be determined using eq 1,¹³ where r_p is the probe radius and a is the pore radius.

$$\frac{d}{\sqrt{r_p a}} \gg 1 \quad (1)$$

For a typical nanopipette probe ($r_p \sim 75$ nm) and nanopores present in membranes ($a \sim 150$ and 250 nm) used in this study, the requirements of a noninteracting probe are satisfied at probe–sample distances of $d \gg 106$ nm for the 300 nm diameter nanopore membrane and $d \gg 137$ nm for the 500 nm diameter nanopore membrane.

Equation 1 also implies a greater probe–sample distance results in smaller perturbation of the diffusion field. Increasing the probe–sample distance, however, will lower the resolution for both topographic and ion current images. To compromise these two requirements, accurate current measurements and high-resolution images, a probe–sample separation of ca. 300 nm was maintained by selecting a set-point equal to $\sim 1\%$ of the maximum modulated ion current (Figure 7). At this working distance, SICM can achieve optimal imaging capability²⁸ and the criterion of a noninteracting probe can be satisfied.

An additional caveat lies in the distance-modulated feedback mode of SICM employed in these experiments. Distance-modulation feedback results in physical modulation of the nanopipette probe in the vertical (Z) dimension, a feature typically not encountered in SECM experiments. This modulation results in convection in the proximity of the probe, a potential source of perturbation which is not accounted for in the simple model described here. (Possible implications of modulation-induced convection will be discussed further *vide infra*.)

Modeling Diffusion through a Nanopore. A simple model can be constructed to aid in evaluation of the experimental results. This model must account for the concentration of ions at a given coordinate (probe position), especially in the vicinity of pores in the nanopore membrane, where the concentration of ions is determined by the transmembrane concentration difference employed. Considering a nanopore in the membrane as a hemispherical source of ions with radius equal to the radius of the nanopore affords a suitable model for further quantifying our observations. It should be noted that models based on the true geometry, a disk-shaped source, are more accurate than the hemispherical approximation. At moderate distances from the pore opening, however, the simpler hemispherical model proves adequate.¹³

As reported previously, the concentration profile of a hemispherical source can be described in Cartesian coordinates by eq 2 in which the plane parallel to the surface of the membrane is defined as the X – Y plane, and the Z -axis is defined as perpendicular to the membrane surface.¹³ In eq 2, C_s represents the concentration of sample at the pore opening,¹³ and $C(x)$ is the concentration profile at a displacement of x from a pore opening of radius a , with a Z displacement equal to d .³⁸

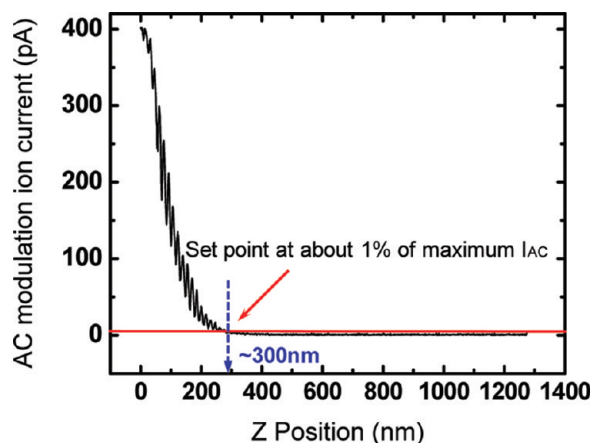
$$C(x) = \left(\frac{2a}{\pi \sqrt{x^2 + d^2}} \right) C_s \quad (2)$$

(38) Piper, J. D.; Clarke, R. W.; Korchev, Y. E.; Ying, L. M.; Klenerman, D. *J. Am. Chem. Soc.* **2006**, *128*, 16462–16463.

Table 1. Summarized Ion Current Measurements for 300 and 500 nm Diameter Nanopore Membranes at Indicated Transmembrane Concentration Differences^{a,b}

KCl concentration (M) (upper/lower chamber)	300 nm diameter nanopore membrane		500 nm diameter nanopore membrane	
	nanopipette 1 ion current (pA)	nanopipette 2 ion current (pA)	nanopipette 3 ion current (pA)	nanopipette 4 ion current (pA)
0.1/0.1	7.7 ± 0.7	7.0 ± 0.5	21.7 ± 2.2	19.3 ± 1.5
0.1/0.5	13.9 ± 0.8	12.1 ± 0.5	45.3 ± 5.4	37.3 ± 2.3
0.1/1.0	20.2 ± 0.6	16.4 ± 0.3	62.2 ± 2.4	55.3 ± 1.5
0.1/2.0	36.0 ± 0.9	34.3 ± 0.1	114.7 ± 5.8	89.3 ± 1.2
0.1/4.0	56.1 ± 0.5	53.6 ± 3.2	157.9 ± 10.0	152.8 ± 3.3

^a Standard deviations calculated from ≥ 5 measurements. ^b Data sets for two nanopipettes are shown for each membrane to illustrate the differences which may arise from nanopipettes used.

**Figure 7.** Typical current–distance curve for a 150 nm diameter nanopipette approaching a surface.

With the use of this equation, concentrations of ions which determine the magnitude of ion current measured by a nanopipette at lateral distance x and height d from a hemispherical ion source of radius a can be calculated.

To estimate the ion current through a permeable membrane in the presence of both a transmembrane concentration difference and an applied potential difference, the Poisson–Nernst–Planck (PNP) theory may be employed. Use of the PNP equations typically requires a numerical solution. By ignoring mobile ion–mobile ion interactions and using a linear potential drop model to describe the potential gradient across the channel (pore) in the membrane, the solution of the PNP equations can be simplified to the well-known Goldman–Hodgkin–Katz (GHK) model.³⁹ For a system with a porous membrane immersed in a monovalent solution, such as KCl, the GHK model describes the flux, j , of $+/-$ ions through a pore with eq 3, where D is the diffusion coefficient, L is the length of the pore (which is equal to the thickness of the membrane), C_s^L and C_s^U are the bulk concentrations of electrolyte in the lower chamber and upper chamber, respectively, and Δ is equal to $e_0\phi_{app}/kT$, where e_0 is proton charge, ϕ_{app} is the applied potential across the membrane, k is Boltzmann's constant, and T is the absolute temperature.³⁹

$$j_{\pm} = \frac{\mp D_{\pm} \Delta}{L} \left(\frac{C_s^L}{1 - e^{\mp \Delta}} - \frac{C_s^U}{e^{\pm \Delta} - 1} \right) \quad (3)$$

(39) Chung, S.-H., Anderson, O. S., Krishnamurthy, V., Eds. *Biological Membrane Ion Channels: Dynamics, Structure, and Application*; Springer: New York, 2007.

From eq 3, it is obvious that the magnitude of the ion flux is influenced by the concentration of ions present on either side of the membrane. Furthermore, ions emerging from a pore establish a nonhomogeneous concentration profile, and the effective concentration, $C(x)$, which contributes to the flux, is a function of radial distance away from a pore, as is described by eq 2. To evaluate this nonuniform concentration profile, we replace bulk concentrations, C_s^L and C_s^U , in eq 3 with a positional dependence term arrived at by multiplying each concentration by the factor $[2a]/[\pi(x^2 + d^2)^{1/2}]$ (cf. eq 2). From this, we obtain a formula describing the position dependence of ion flux emanating from the nanopore.

$$j_{\pm}(x) = \left(\frac{2a}{\pi\sqrt{x^2 + d^2}} \right) \frac{\mp D_{\pm} \Delta}{L} \left(\frac{C_s^L}{1 - e^{\mp \Delta}} - \frac{C_s^U}{e^{\pm \Delta} - 1} \right) \quad (4)$$

The flux, j , is converted to the current, i , by considering Faraday's constant as well as the cross-sectional area of the pore (πa^2), giving eqs 5 and 6 (see the Supporting Information).

$$i_{\pm}(x) \cong \mp 1000 \pi a^2 \left(\frac{2a}{\pi\sqrt{x^2 + d^2}} \right) \frac{D_{\pm} \Delta}{L} \left(\frac{C_s^L}{1 - e^{\mp \Delta}} - \frac{C_s^U}{e^{\pm \Delta} - 1} \right) \quad (5)$$

$$\cong \mp 1000 \left(\frac{2a^3}{\sqrt{x^2 + d^2}} \right) \frac{D_{\pm} \Delta}{L} \left(\frac{C_s^L}{1 - e^{\mp \Delta}} - \frac{C_s^U}{e^{\pm \Delta} - 1} \right) \quad (6)$$

The experimental measurement of current magnitude is a contribution of both positive and negative ions; the total ion current across a pore, I , is thus calculated by subtracting the negative ion current i_- from the positive ion current i_+ .

$$I = i_+ - i_- \quad (7)$$

Using the ion current calculated from eq 7 and inputting the experimental conditions (see the Supporting Information) used in this study, we obtain a model which describes the ion current as a function of the transmembrane concentration difference of ions, the applied transmembrane potential, the pore geometry, and the probe (nanopipette) displacement over a pore in a membrane. Before going further, we must clarify that estimates for the contribution of the electrical field to the ion current

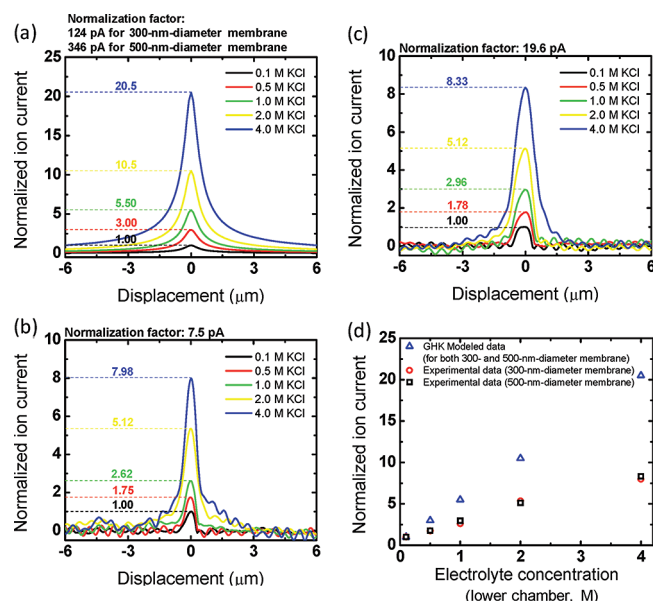


Figure 8. (a) GHK-modeled two-dimensional ion current profiles over a single pore for both 300 and 500 nm diameter nanopore membranes. Experimental ion current profiles for a single pore in (b) 300 and (c) 500 nm diameter nanopore membranes under specified transmembrane concentration differences are also presented. Normalization factors indicated are the peak current values recorded for the transmembrane concentration difference of 0.1 – 0.1 M KCl. (d) Normalized modeled (Δ) and experimental (\circ and \square) ion currents are plotted as a function of the KCl concentration in the lower chamber.

described here consider the potential applied across a single pore in the membrane, instead of across the entire membrane. Such a simplification is valid, as the SICM probe is very close to the membrane and can measure the localized ion current through an individual pore at small probe–sample separations, as opposed to the ion current through the entire membrane area.²⁹ In this situation, the effective applied voltage ϕ_{app} used to obtain Δ is calculated according to Ohm's law by considering the resistances of the nanopipette and a single pore linked in series. In comparison with these two resistances (the resistances of the nanopipette and of the pore), the potential drop across the electrolyte is considered negligible. The resistances of individual pores used in this study are estimated by measuring the current–voltage response of these porous membranes (see the Supporting Information).

Figure 8 shows the calculated (Figure 8a) and experimental two-dimensional ion current profiles over a single pore for both 300 (Figure 8b) and 500 (Figure 8c) nm diameter membranes, measured for each transmembrane concentration difference. To facilitate comparison between modeled and experimental results, ion currents are normalized to the peak current at zero transmembrane concentration difference (i.e., 0.1 M (upper chamber) – 0.1 M (lower chamber)), where effects of the concentration difference on the ion current are minimized, reducing potential sources of error. For each set of current profiles, the normalization factor (i.e., the peak current value observed for a transmembrane concentration difference of 0.1 M (upper chamber) – 0.1 M (lower chamber)) is indicated above each plot. Interestingly, when

normalized and plotted, the modeled current profiles (Figure 8a) for pores of different size are identical (normalization factors of modeled data are 124 and 346 pA for 300 and 500 nm diameter nanopores, respectively). For modeled data (Figure 8a), normalized current profiles show Gaussian shapes with peak values of 1.00, 3.00, 5.50, 10.5, and 20.5, corresponding to KCl concentrations of 0.1, 0.5, 1.0, 2.0, and 4.0 M in the lower chamber, respectively. The normalized experimental current profiles of the 300 (Figure 8b) and 500 (Figure 8c) nm diameter nanopore membranes also approximate Gaussian shapes with a higher normalization factor (19.6 pA) for 500 nm diameter nanopore membranes. When compared as normalized peak current values, results for the 300 and 500 nm diameter nanopore membranes obtained at the same transmembrane concentration difference match very well, as predicted by the GHK model. These results suggest no matter what pore size is used, normalized ion current magnitude is proportional to the transmembrane concentration difference.

Interpreted in terms of normalized ion currents, modeled data (Figure 8d, Δ) are typically larger than experimental data (Figure 8d, \circ and \square). Furthermore, the deviation between the model and experiment becomes larger as the transmembrane concentration difference becomes greater. In other words, this deviation becomes more pronounced as the transmembrane concentration difference changes from 0.1 M (upper chamber) – 0.1 M (lower chamber) to 0.1 M (upper chamber) – 4.0 M (lower chamber). In the simple model described here, several assumptions or sources of error are present which might contribute to this discrepancy between normalized experimental and modeled peak current at the same transmembrane concentration difference.

One possible source of deviation between the model and experiment is convection caused by the vertical modulation of the nanopipette. We have attempted to avoid this by choosing a suitable distance from the pore of the membrane. However, on the basis of the trend observed, it is possible that convection still contributes to observed deviations between normalized experimental and modeled current values. When ion currents arising from higher concentration differences are measured, a higher concentration difference between the upper and lower chambers of the diffusion cell results in spatial variations in the concentration profile which are steeper. Thus, convection induced by vertical modulation of the nanopipette (± 50 nm vertical displacement) perturbs the concentration to a higher degree when a higher concentration difference is employed. If convection is responsible for deviations between the experimental and modeled results, a larger effect will be observed when the concentration difference is greater in agreement with the trend shown in Figure 8d.

Assumptions are also present in the GHK approximation of the PNP equations. These assumptions include ignoring mobile ion–mobile ion interactions. It is known that interactions between ions should be greater for higher concentrations,⁴⁰ which would result in deviations at higher concentrations of KCl, as observed here. A second assumption of the GHK model used to predict the ion current emanating from the pore is a

(40) Lakshminarayanaiah, N. *Equations of Membrane Biophysics*; Academic Press, Inc.: Orlando, FL, 1984.

linear potential drop within the pore. This assumption should be relatively accurate for symmetric cylindrical pores such as those used here. In fact, recent theoretical models of nanoscale channels have predicted quite linear potential profiles for cylindrical nanopores 1–2 orders of magnitude smaller than we examine here.⁴¹ Also, the same trend is observed for the 300 and 500 nm diameter nanopore membrane which suggests an alternate origin of the observed discrepancies.

There are also well-known permselectivities exhibited as pores approach smaller dimensions, which may cause overall currents to differ from ideal values. Permselectivities exist in the SICM nanopipette probe, especially when the asymmetric nature and surface charge of the nanopipette tip are considered.⁴² For the nanopipettes and the ion concentrations used here (0.1 M KCl in the nanopipette), the current–voltage response of the nanopipette is rectified over the applied potential range of ± 1 V, with higher currents passed at negative biases with respect to the corresponding positive bias (see the Supporting Information). This indicates substantial permselectivity exists in the nanopipette, with cations passed preferentially to anions as described previously.⁴³ Measurements presented here, however, were performed at an applied potential difference of +100 mV. For typical nanopipettes over the potential range of ± 200 mV, the current–voltage response is linear and no significant rectification is observed.

An additional possibility which could lead to the observed discrepancy of trends between modeled and experimental results is surface conductance. The nanopores present in the membranes studied and the nanopipette probes used both possess a negative surface charge (nominally 0.5 e/nm^2 ⁴⁴ for glass and 1.7 e/nm^2 ⁴⁵ for the polyimide nanopores) which can give rise to substantial ion currents which are not described by the GHK-based model we employ. Surface conductance leads to a substantial deviation from bulk solution conductivities, especially with respect to nanopore structures with high surface to volume ratios.⁴⁴ The effect of surface conductance is also exaggerated as the ionic strength of the electrolyte solution employed is lowered.⁴⁴ This leads to higher than expected conductivities for nanopore structures operated in dilute ionic strength solutions. For example, previous reports using rectangular nanochannels have demonstrated surface conductance can play a significant role (with respect to deviation from bulk conductances) as one pore dimension becomes small (e.g., ≤ 100 nm) or at low ionic strengths (e.g., ≤ 0.1 M).⁴⁴ For the porous membranes studied here, however, pore diameters are larger than 100 nm (~ 300 and ~ 500 nm, respectively) and ionic strengths were significant (0.1 M or greater), suggesting contributions from surface currents in the nanopores of the membrane are minimal.

Surface conductivity can also contribute to the currents present in the nanopipette.^{46,47} The resistance of a nanopipette in the absence of any surface conductivity can be estimated by

eq 8⁴⁷ where Γ is the resistance of a pipette, γ is the specific resistance of the electrolyte filled in the pipette, θ is the cone angle of the pipette tip, and r is the radius of the pipette tip opening. For nanopipettes used here, with a nominal tip opening of 150 nm ($r = 75$ nm) and a cone angle (θ) of 13.3° (both measured via SEM), when filled with 0.1 M KCl (measured specific resistance, γ , $80.13 \Omega \cdot \text{cm}$) the resistance of $\sim 277 \text{ M}\Omega$ is calculated for our nanopipettes. In comparison to the measured resistance of the nanopipettes used ($\sim 119 \text{ M}\Omega$, see the Supporting Information), this number, $\sim 277 \text{ M}\Omega$, underestimates conductivity of the electrolyte filled in nanopipette. Therefore, surface conductivity indeed contributes to reduce the resistance of the nanopipette (from ~ 277 to $\sim 119 \text{ M}\Omega$) and deviations between the experimental and modeled results are expected to become more pronounced at lower ionic strength. To account for possible effects of surface conductivity on the true resistance of nanopipettes into the GHK model, we use the experimentally measured resistance of the nanopipette to calculate modeled ion currents. As analyzed here, however, we observe greater deviations as the ionic strength of the electrolyte increases, opposite to the expected tendency—greater deviations as the ionic strength decreases. This suggests that the contribution of surface conductivity to nanopipette resistance is not responsible for the observed discrepancies between normalized modeled and experimental data.

$$\Gamma \cong \frac{\gamma \cot(\theta/2)}{\pi r} \quad (8)$$

Finally, the use of a hemispherical model versus a true disk-shaped source adds an intrinsic error at small probe–sample separations, as described previously.¹³ Thus, taken together, there are several possible sources of the observed discrepancy between the modeled and theoretical trends observed. We are presently developing a more detailed description to increase the fidelity of the model and our ability to predict ion currents.

Even though the trend in ion current profiles estimated with the GHK model fit the experimental data reasonably well with respect to the normalized peak current values, there is a distinct difference between the absolute experimental and model current values listed in Table 2. In this table, the collection efficiency ε is defined by eq 9, where i_G is the theoretical maximum ion current estimated with GHK model and i is the experimental ion current measured with SICM.

$$\varepsilon (\%) = \frac{i}{i_G} \times 100 \quad (9)$$

From Table 2, for either the 300 or 500 nm diameter nanopore membrane, the collection efficiency range is 2–6%. This implies not all of the ion current emerging from the pore is measured at the 150 nm diameter tip opening of the nanopipette. Under conditions studied here, the low collection efficiencies observed indicate a fraction of the total ion current through a pore is detected by a scanning nanopipette.

(41) Vlassiuk, I.; Smirnov, S.; Siwy, Z. *Nano Lett.* **2008**, *8*, 1978–1985.

(42) Ying, L. M.; White, S. S.; Bruckbauer, A.; Meadows, L.; Korchev, Y. E.; Klennerman, D. *Biophys. J.* **2004**, *86*, 1018–1027.

(43) Wei, C.; Bard, A. J.; Feldberg, S. W. *Anal. Chem.* **1997**, *69*, 4627–4633.

(44) Stein, D.; Kruithof, M.; Dekker, C. *Phys. Rev. Lett.* **2004**, *93*, 035901.

(45) Fulinski, A.; Kosinska, I.; Siwy, Z. *New J. Phys.* **2005**, *7*, 132.

(46) Clarke, R. W.; Piper, J. D.; Ying, L. M.; Klennerman, D. *Phys. Rev. Lett.* **2007**, *98*, 198102.

(47) Lavalie, M.; Schanne, O. F.; Hebert, N. C., Eds. *Glass Microelectrodes*; John Wiley and Sons, Inc.: New York, 1969.

Table 2. Experimental and Modeled Ion Currents for Transmembrane Concentration Ratios Indicated^a

transmembrane concentration ratio (C_s^L/C_s^U)	300 nm diameter nanopore membrane			500 nm diameter nanopore membrane		
	experimental current (pA)	theoretical current (pA)	collection efficiency (%)	experimental current (pA)	theoretical current (pA)	collection efficiency (%)
1	7.3 ± 0.7	124	5.9	20.5 ± 1.4	346	5.9
5	13.0 ± 1.1	373	3.5	41.3 ± 3.7	1037	3.9
10	18.3 ± 2.1	684	2.7	58.8 ± 4.5	1901	3.1
20	35.2 ± 1.1	1306	2.7	102.0 ± 9.4	3630	2.8
40	54.9 ± 2.4	2550	2.2	155.3 ± 6.1	7087	2.2

^a Standard deviations calculated from ≥10 measurements.

CONCLUSION

Analysis of the localized ion transport through nanopores as presented here demonstrates the capability of SICM to correlate topographic information with nanoscale transport properties. Instead of common topographic features, ion current images taken by SICM can be used to discern the transport pathways for porous materials. In addition, the dependence of the ion current magnitudes on the transmembrane concentration differences displays a proportional relationship. GHK theory has been used to model the ion current emanating from the pore and the distance-dependent current profiles produced. These models fit reasonably well with experimental measurements with respect to normalized current values. A number of potential sources for observed deviations between the experimental and modeled data have been discussed, including surface conductivity of the nanopipette and convective contributions arising from the distance modulation of the tip.

On the basis of the analysis presented, further studies of nanoscale transport properties, e.g., ion flux, surface conductivity, and permselectivity, are clearly warranted. We are presently developing a more inclusive model to predict observed currents with greater fidelity.

ACKNOWLEDGMENT

Research was supported by the American Heart Association and Indiana University.

SUPPORTING INFORMATION AVAILABLE

Additional information as noted in text. This material is available free of charge via the Internet at <http://pubs.acs.org>.

Received for review January 9, 2009. Accepted April 20, 2009.

AC900065P